Kinetic Modeling of 3′-Deoxy-3′-^{18}F-Fluorothymidine for Quantitative Cell Proliferation Imaging in Subcutaneous Tumor Models in Mice

Su Jin Kim[1–4], Jae Sung Lee[1–4], Ki Chum Im[5,6], Seog-Young Kim[5,6], Soo-Ah Park[5,6], Seung Jin Lee[5,6], Seung Jun Oh[5,6], Dong Soo Lee[1–4], and Dae Hyuk Moon[5,6]

[1]Department of Nuclear Medicine, College of Medicine, Seoul National University, Seoul, Korea; [2]Department of Biomedical Sciences, College of Medicine, Seoul National University, Seoul, Korea; [3]Interdisciplinary Programs in Radiation Applied Life Science, College of Medicine, Seoul National University, Seoul, Korea; [4]Institute of Radiation Medicine, Medical Research Center, Seoul National University, Seoul, Korea; [5]Department of Nuclear Medicine, Asan Medical Center, University of Ulsan College of Medicine, Seoul, Korea; and [6]Institute for Innovative Cancer Research, Asan Medical Center, Seoul, Korea

3′-Deoxy-3′-^{18}F-fluorothymidine (^{18}F-FLT) is a thymidine analog that was developed for measuring tumor proliferation with PET. The aim of this study was to establish a kinetic modeling analysis method for quantitative ^{18}F-FLT PET studies in subcutaneous tumor models in mice. **Methods:** To explore the validity of an image-derived left ventricular input function, we measured equilibrium constants for plasma and whole blood and metabolite fractions in blood after ^{18}F-FLT injection. In parallel, dynamic ^{18}F-FLT PET scans were acquired in 24 mice with a small-animal dedicated PET scanner to compare arterial blood activities obtained by PET and blood sampling. We then investigated kinetic models for ^{18}F-FLT in human epithelial carcinoma (A431) and Lewis lung carcinoma tumor models in mice. Three-compartment models with reversible phosphorylation ($k_4 \neq 0$, 3C5P) and irreversible phosphorylation ($k_4 = 0$, 3C4P) and a 2-compartment model (2C3P) were examined. The Akaike information criterion and *F* statistics were used to select the best model for the dataset. Gjedde–Patlak graphic analysis was performed, and standardized uptake values in the last frame were calculated for comparison purposes. In addition, quantitative PET parameters were compared with Ki-67 immunostaining results. **Results:** ^{18}F-FLT equilibrated rapidly (within 30 s) between plasma and whole blood, and metabolite fractions were negligible during PET scans. A high correlation between arterial blood sampling and PET data was observed. For 120-min dynamic PET data, the 3C5P model best described tissue time–activity curves for tumor regions. The net influx of ^{18}F-FLT (K_{FLT}) and k_3 obtained with this model showed reasonable intersubject variability and discrimination ability for tumor models with different proliferation properties. The K_{FLT} obtained from the 60- or 90-min data correlated well with that obtained from the 120-min data as well as with the Ki-67 results. **Conclusion:** The image-derived arterial input function was found to be feasible for kinetic modeling studies of ^{18}F-FLT PET in mice, and kinetic modeling analysis with an adequate compartment model provided reliable kinetic parameters for measuring tumor proliferation.

Key Words: 3′-deoxy-3′-^{18}F-fluorothymidine (^{18}F-FLT); cellular proliferation; kinetic modeling; arterial input function

J Nucl Med 2008; 49:2057–2066
DOI: 10.2967/jnumed.108.053215

The thymidine analog 3′-deoxy-3′-^{18}F-fluorothymidine (^{18}F-FLT) is used to assess rate-controlling enzyme thymidine kinase 1 (TK1) activity in the DNA salvage pathway and hence cellular proliferation (*1,2*). Compared with ^{11}C-thymidine, ^{18}F-FLT offers the advantages of a longer physical half-life and the generation of few metabolites in vivo. Furthermore, because it is not incorporated into DNA, ^{18}F-FLT is trapped in cells like ^{18}F-FDG (*3*).

For quantifying ^{18}F-FLT uptake in vivo, simple semiquantitative methods, such as determination of the standardized uptake value (SUV) and model-independent graphic analysis, have been shown to be useful for assessing ^{18}F-FLT metabolism (*4–7*). However, compartmental modeling is necessary to fully characterize the kinetics of ^{18}F-FLT uptake into tissue (*8*). Several investigations of ^{18}F-FLT kinetic modeling in humans have been performed (*6,8–13*). In vivo imaging studies of experimental cancer models in mice have provided important means of understanding the mechanisms of cancer progression and of assessing the therapeutic effects of newly developed drugs (*14–17*). Serial ^{18}F-FLT PET studies of the monitoring of tumor response to radiotherapy or antiproliferative treatment (*3,7,18–20*) in various tumor models have been performed. However, only semiquantitative approaches were used to assess the relationship between

Received Apr. 8, 2008; revision accepted Aug. 18, 2008.
For correspondence or reprints contact: Jae Sung Lee, Departments of Nuclear Medicine and Biomedical Sciences, College of Medicine, Seoul National University, 28 Yungun-Dong, Chongno-Gu, Seoul 110-744, Korea.
E-mail: jaes@snu.ac.kr

changes in ^{18}F-FLT uptake and therapeutic responses in these studies.

In mice, left ventricular (LV) activity can be used as an image-derived input function for quantifying ^{18}F-FLT metabolism because no ^{18}F-FLT metabolites are found in plasma, but the data so derived need to be validated. Therefore, in this study, we explored the validity of an image-derived LV input function in mouse ^{18}F-FLT PET and investigated kinetic models for ^{18}F-FLT in mice bearing human epithelial carcinoma (A431) and Lewis lung carcinoma (LLC) tumors.

MATERIALS AND METHODS

Radiopharmaceutical Preparation

^{18}F-FLT was prepared from 5′-*O*-(DMTr-2′-deoxy-3′-*O*-nosyl-β-D-threopentafuranosyl)-3-*N*-BOC-thymine as a precursor by the nucleophilic fluorination of ^{18}F-fluoride with a protic solvent (*t*-butanol or *t*-amyl alcohol) (*21*). Typically, decay-corrected radiochemical yields ranged from 60% to 70%, and after high-performance liquid chromatography (HPLC) purification, the radiochemical purity was 98% ± 1.2% (mean ± SD). The specific activity of the ^{18}F-FLT obtained was greater than 100 TBq/mmol.

Cell Cultures and Tumor Models

A431 and LLC cell lines were obtained from the American Type Culture Collection. Cells were routinely cultured in Dulbecco's modified Eagle medium supplemented with 10% heat-inactivated fetal bovine serum (FBS), L-glutamine (2 mM), penicillin (100 IU/mL), and streptomycin (50 g/mL) (Gibco, Invitrogen Corp.). Cells were maintained at 37°C in an atmosphere of 5% CO_2 in air.

BALB-c/nu and C57BL/6 mice (both from Charles River Laboratories) subcutaneously injected with A431 and LLC cells, respectively, were used as tumor models. The research protocol used was approved by the Institutional Animal Care and Use Committee at the Asan Institute for Life Science. Mice were also maintained in accordance with guidelines issued by this committee. Exponentially growing 7×10^6 A431 and 1×10^6 LLC cells suspended in 300 μL of the culture medium described earlier were injected subcutaneously into the right forelimbs of anesthetized mice. When tumor diameters reached 6–10 mm at 10–12 d after injection, mice were used for the experiments.

Thymidine Kinase Assay

Thymidine kinase activities were measured in A431 and LLC tumors excised from 3 and 4 mice, respectively, that were treated in parallel with animals used for imaging. The activities were measured with a previously described thymidine kinase assay that was slightly modified (*1*). In brief, tumors were lysed in lysis buffer and incubated for 30 min on ice. Lysates were centrifuged at 10,000*g* for 20 min at 4°C, and supernatants were recentrifuged at 100,000*g* for 1 h at 4°C to separate mitochondrial fractions. After protein contents were determined, cytosolic fractions were assayed for thymidine kinase activities in a reaction buffer containing 10 M ^{3}H-thymidine (TRK120; 925×10^9 Bq/mmol; Amersham Bioscience). Mixtures were then incubated at 37°C with gentle stirring, and samples were removed and added to 10 mM ethylenediaminetetraacetic acid to stop the reaction. For sequestration of labeled nucleotides, samples were spotted onto DE-81 filters (Whatman), dried, and washed in 4 mM ammonium formate and 95% ethanol. Radioactivity was measured by liquid scintillation counting with Ultima Gold F scintillation cocktail solution (Perkin-Elmer). Activities were calculated with linear time–activity curves and are presented as picomoles of phosphorylated thymidine per minute per milligram of protein. TK1 activities (mean ± SD) in A431 and LLC tumors were 0.074 ± 0.023 and 0.028 ± 0.01 pmol of phosphorylated thymidine per minute per milligram of protein, respectively; these values were significantly different ($P < 0.05$).

PET Scans

PET scans were performed by use of a microPET Focus120 system (Siemens Medical Solutions, Inc.) with resolutions of 1.18 mm (radial), 1.13 mm (tangential), and 1.44 mm (axial) at the center of the field of view (*22*). A 37-frame dynamic protocol (4×3 s, 6×1 s, 7×6 s, 8×30 s, 1×300 s, and 11×600 s) was used for the emission PET scans. Mice were maintained under isoflurane anesthesia during the scans, and body temperatures were maintained at 36°C with an electric heating pad. Animals fasted for 4 h before imaging. Transaxial images were reconstructed as $128 \times 128 \times 95$ matrices of $0.432 \times 0.432 \times 0.796$ mm by use of a filtered back-projection algorithm with a Hamming filter at a cutoff frequency of 0.5 cycle per pixel.

Validation of LV Input Function

Forty-four normal C57BL/6 mice were studied to verify the LV input function derived from dynamic PET data. For measurement of the equilibrium constant for plasma and whole blood over time, arterial blood samples were obtained from 16 mice by cardiac puncture at 30 s, 2 min, 5 min, and 10 min (4 mice at each sampling time point) after injection of 37 MBq of ^{18}F-FLT. Arterial blood was collected in heparinized tubes from the LV cavity by direct cardiac puncture. Immediately after sample collection, plasma was separated from whole blood by centrifugation at 10,000*g* for 20 s at 4°C. The plasma samples (>15 μg) were weighed with 0.1-mg precision. Counts in the plasma and whole-blood samples were determined with a well γ-counter (COBRA II Auto Gamma; Canberra Packard). All tubes were incubated at 4°C before use. The time interval between plasma sampling after centrifugation and the sacrifice of the animal was 53 ± 11 s.

Dynamic PET scans were performed in 24 mice to compare arterial blood activities obtained by PET with activities obtained from blood data. The 24 animals were divided into 4 equal groups according to the time of arterial blood sampling (5, 10, 30, and 60 min after the initiation of scanning). Dynamic PET scans were started immediately after the injection of 37 MBq of ^{18}F-FLT into tail veins and were completed at each group time for blood sampling by direct cardiac puncture. Arterial blood samples (20 μl) were analyzed with the well γ-counter.

Cross-calibration factors for the well γ-counter and PET scanner were independently measured with a mouse-size uniform cylindric phantom (diameter = 3 cm, length = 11.5 cm) filled with 37 MBq of ^{18}F-FLT solution. To obtain a PET image–derived input function, cylindric volumes of interest (VOIs) (length of 3 slices) were drawn on the centers of the left ventricles on PET images. The diameters of these cylindric VOIs were varied from 1.3 to 3.0 mm (3–7 pixels in diameter) to explore the effects of VOI size on the image-derived input function. Finally, correlation analysis was performed on cross-calibrated counts from arterial blood and image-derived input functions. The ratios of cross-calibrated PET image–derived and blood sample–derived activities (recovery coefficients) were also calculated, and the reciprocal of the mean ratio of the data for the 24 imaged animals (at all time points between 5 and 60 min) was used

as a partial-volume effect correction factor for the image-derived input function.

^{18}F-FLT Metabolite Analysis

Metabolite fractions in arterial blood were measured at 1 and 2 h after the injection of 185 MBq of ^{18}F-FLT into 4 mice as described previously (*3*). Plasma samples were deproteinated by the addition of ice-cold acetonitrile and centrifugation (1,800*g*, 10 min). Supernatants containing ^{18}F-FLT and metabolites were passed through a sterile filter (0.2 μm) and analyzed by HPLC. Eluted material was monitored with a radioactivity detector, and unchanged phosphorylated ^{18}F-FLT fractions were determined by HPLC with radioisotope detectors.

Metabolite fractions in tumors were also measured immediately after dynamic imaging studies as described later. Tumor samples were cut into small pieces and homogenized. Supernatants obtained by centrifugation were filtered and analyzed as described earlier.

Kinetic Modeling

For kinetic modeling studies, PET scans were performed on 19 mice bearing A431 (n = 9) and LLC (n = 10) tumors. Dynamic emission scans were acquired after the injection of 30–46 MBq of ^{18}F-FLT into tail veins, and scanning was continued for 2 h.

To obtain time–activity curves for kinetic analysis, cylindric VOIs with a diameter of 3.0 mm and a length of 3 slices were drawn on PET images. LV time–activity curves corrected for partial-volume effects with the correction factor described earlier were used as the input function. Tissue time–activity curves were obtained from tumor-bearing regions on the right forelimbs and from normal contralateral regions.

Compartmental Analysis

To determine the optimal compartmental model for ^{18}F-FLT in mice, we tested a 3-compartment model suggested for human data (*8,9*) and its nested models. Figure 1 shows the 3-compartment model, in which the parameters K_1, k_2, k_3, and k_4 represent the rate of transport from plasma to tissue, the rate of outflow from tissue to plasma, the TK1 phosphorylation rate, and the dephosphorylation rate, respectively. The blood volume fraction (V_b) was included in the modeling, and 3-compartment models with reversible phosphorylation ($k_4 \neq 0$, 3C5P) and irreversible phosphorylation ($k_4 = 0$, 3C4P) were examined. In addition, a 2-compartment model that combined exchangeable and phosphorylated compartments into a single tissue compartment with 3 parameters (2C3P: K_1, k_2, and V_b) was also considered.

The PMOD software package (version 2.65; PMOD Group (*23*)) was used for parameter estimation. Tissue time–activity curves were fitted to the models by use of the nonlinear least-squares method with the Levenberg–Marquardt algorithm, which minimizes the weighted sum of squared errors between PET measurements and model solutions. Inverse SDs of frame counts were used as weights. Estimated parameters were restricted to the following value ranges: 0.0–0.5 for K_1, 0.0–5.0 for K_1/k_2, 0.0–1.0 for k_3, 0.0–0.5 for k_4, and 0.0–0.2 for V_b. Initial values for these parameters were set at 0.1, 1.0, 0.1, 0.01, and 0.05 for A431 and at 0.1, 0.5, 0.01, 0.01, and 0.05 for LLC, respectively.

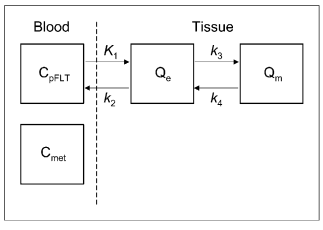

FIGURE 1. Kinetic model for ^{18}F-FLT. C_{pFLT} represents concentration of ^{18}F-FLT in arterial plasma. Tissue is composed of exchangeable tissue compartment (Q_e) and compartment of trapped phosphorylated ^{18}F-FLT nucleotides (Q_m). Parameters K_1 and k_2 are rate constants for forward and reverse transport of ^{18}F-FLT between plasma and tissue pool, respectively. Rate constants for precursor and phosphorylated ^{18}F-FLT denote thymidine kinase–mediated phosphorylation (k_3) and dephosphorylation (k_4) of ^{18}F-FLT. C_{met} = concentration of metabolites in arterial plasma.

The net influx of ^{18}F-FLT (K_{FLT}), the total distribution volume (DV_{tot}), and the distribution volume for phosphorylated ^{18}F-FLT nucleotides (DV_m) were estimated as follows:

$$K_{FLT} = \frac{K_1 k_3}{k_2 + k_3} \quad DV_{tot} = \frac{K_1}{k_2}\left(1 + \frac{k_3}{k_4}\right) \quad DV_m = \frac{K_1 k_3}{k_2 k_4}.$$

We chose an adequate compartment model on the basis of the Akaike information criterion (AIC) and the F test. We also examined the correlations between kinetic parameters (such as K_{FLT}, DV_{tot}, and DV_m) obtained with the best model and percentages of Ki-67–positive nuclei (% Ki-67). Kinetic parameters obtained with simpler methods (fewer parameters or a shorter scan duration) were compared with those obtained with the best model and data acquired over 120 min.

Nonparametric or Semiquantitative Approaches

Gjedde–Patlak graphic analysis (GPGA) was also performed to estimate K_{FLT}. Only the linear region on the GPGA plot (A431: 7.5–90 min; LLC: 20–120 min) was included in the linear regression analysis. The SUV at the last frame (duration of 10 min) was also calculated.

Immunohistochemical Analysis

After small-animal PET images were acquired from mice bearing tumors, animals were sacrificed for immunohistochemical analysis. Tumors were fixed with 10% neutral buffered formalin and embedded in paraffin. For Ki-67 immunostaining, 4-μm-thick sections were obtained from paraffin blocks. Paraffin sections were placed on slides, deparaffinized in xylene, and rehydrated in graded ethanol. Endogenous peroxidase was blocked with 3% hydrogen peroxide in 70% methanol for 15 min. Antigen retrieval was performed with 10 mM citrate buffer solution (pH 6.0) for 15 min in a microwave oven, and sections were cooled to room temperature for 20 min. Sections were incubated overnight at 4°C with monoclonal mouse anti–human Ki-67 antibody. Sections were treated with biotinylated Link (LSAB 2 system-HRP kit; Dakocytomation) for 30 min, incubated with streptavidin–horseradish peroxidase (LSAB 2 system-HRP kit) for 30 min at room temperature, and washed. Sections were treated with diaminobenzidine (Dakocytomation) for 5 min, washed with tap water, counterstained with hematoxylin, rewashed, and mounted. For determination of % Ki-67, more than 1,000 cells per slide were counted and scored with a ×40 optical microscope (Leica) by 2 masked observers.

Statistical Analysis

Correlations between % Ki-67 and parameters estimated from PET data were assessed with Spearman nonparametric rank analysis. Correlations between PET kinetic parameters were also assessed with Spearman analysis. The 2-sample t test was used to compare 2-parameter estimates from different tumors. Statistical analyses were performed with SPSS for Windows (SPSS 12.0KO release 12.0.1; SPSS Inc.).

RESULTS

Image-Derived Input Function

^{18}F-FLT equilibrated rapidly between plasma and whole blood, and the ratios of plasma activity to whole-blood activity converged to a constant value (mean ± SD for 30-s data = 1.0 ± 0.1) within 30 s of intravenous injection and did not change with time. Metabolite analysis in plasma revealed only one major peak of parent ^{18}F-FLT, at 2 h after injection. Figure 2 shows the LV input function obtained for a representative mouse with a VOI with a diameter of 1.3 mm (3 pixels), which was the smallest VOI used. We obtained several samples around the initial peaks of LV input functions. Despite the short duration (1 s) of the initial frames, no counting rate fluctuation was observed for these input functions throughout the scans. Initial peak values of image-derived input functions decreased gradually with increasing VOI diameter. However, these differences were not significant up to a VOI diameter of 3 mm (7 pixels).

Figure 3A shows the regression line for the cross-calibrated arterial blood sample data and PET data (timing difference corrected) obtained with a VOI with a 3-mm diameter. We merged the data acquired at all of the time points (5, 10, 30, and 60 min) to obtain the regression line, which had a high correlation ($r > 0.96$) and little bias. Regression lines for all VOIs showed a similar trend. The magnitudes of arterial blood sample data and PET data obtained at each time point with the same VOIs are compared in Figure 3B, in which the data are presented as means ± SEMs. No time-dependent difference between these data was observed.

Figure 3C shows recovery coefficients, which were defined as ratios of PET data and blood sample data (mean ± SD of 0.94 ± 0.12, 0.94 ± 0.11, 0.93 ± 0.11, 0.93 ± 0.10, and 0.92 ± 0.11 for VOIs with diameters of 1.3, 1.7, 2.1, 2.6, and 3 mm, respectively). Coefficients of variation (CVs) were less than 12.5%.

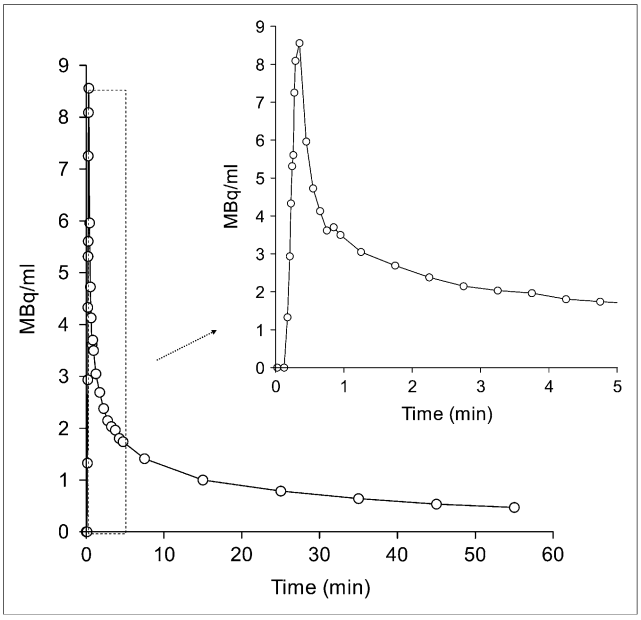

FIGURE 2. Blood time–activity curve generated from VOI (1.3-mm diameter) placed in left ventricle to obtain input function.

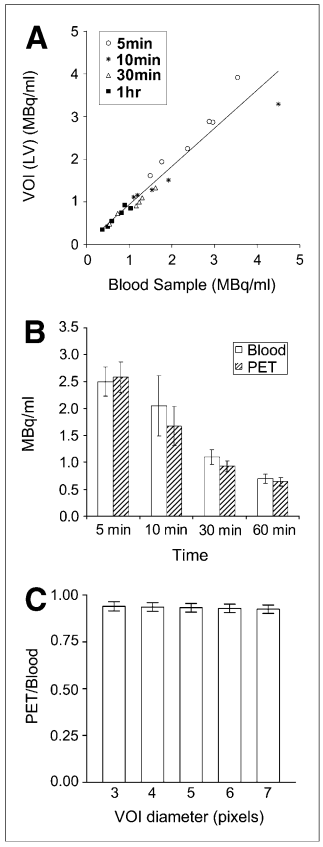

FIGURE 3. Comparison between cross-calibrated arterial blood activities measured by invasive blood sampling and by use of LV VOIs on PET images. (A) High correlation ($r > 0.96$) was observed between arterial blood samples and PET data (VOI diameter = 3 mm). (B) Bar plot of arterial blood samples and PET data obtained from each time point with same VOI. Bars represent means ± SEMs. (C) Mean ratios of PET data and blood sample data were 0.94, 0.94, 0.93, 0.93, and 0.92 for VOIs with diameters of 1.3, 1.7, 2.1, 2.6, and 3 mm, respectively. Input function obtained from VOI with diameter of 3 mm (7 pixels) was divided by 0.92 for kinetic analysis. Bars represent means ± SEMs.

On the basis of these results, the LV time–activity curves obtained with a VOI with a 3-mm diameter (7 pixels) were used as input functions for the kinetic analysis. Input functions were scaled to compensate for differences from blood samples by dividing them by recovery coefficients.

Tissue Time–Activity Curves

Figure 4 shows averaged PET images obtained at 110–120 min after injection and time–activity curves for tumor-bearing and normal regions. Proliferative A431 tumors showed rapid uptake and high ^{18}F-FLT retention (Fig. 4A). On the other hand, LLC tumors had time–activity curves that resembled those of normal regions and had relatively low ^{18}F-FLT retention and rapid clearance (Fig. 4B).

Compartmental Modeling

Time–activity curves were fitted more accurately when the V_b term, which reflected the significant amount of blood activity in VOIs, was included in the model. Means and CVs of kinetic parameters estimated with the 3C5P, 3C4P, and 2C3P models and 120 min of data and K_{FLT} values estimated with GPGA are summarized in Table 1. Data for 2 A431 tumors were excluded from this comparison and from further analyses because tissue time–activity curves

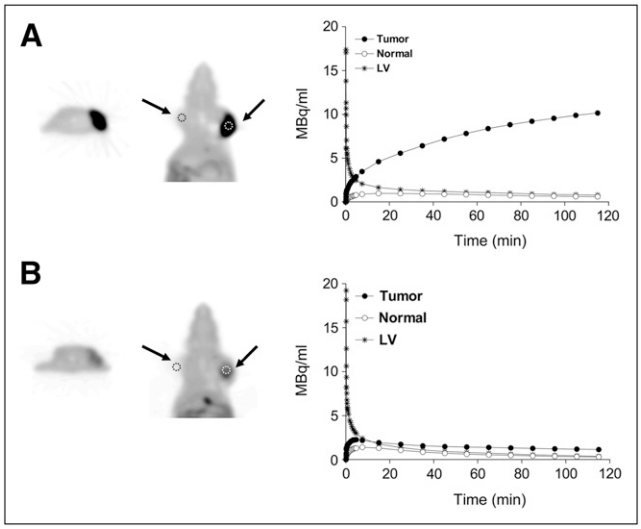

FIGURE 4. Averaged PET images obtained at 110–120 min after injection (representative case for each tumor model). LV input function and tissue time–activity curves were obtained from 3-mm VOIs drawn on tumor-bearing regions (arrows at right) and on contralateral normal tissues (arrows at left) in mice bearing A431 (A) and LLC (B) tumors.

were not properly fitted with the models within physiologically relevant ranges of kinetic parameters, possibly because of motion artifacts. For A431 and LLC tumors, the average ^{18}F-FLT dephosphorylation rates (k_4) were estimated to be 0.011 and 0.015, respectively.

Consistent with the measurable dephosphorylation of phosphorylated ^{18}F-FLT, both tumor cell lines showed the lowest AIC values for all mice when the 3C5P model was used for curve fitting (Table 2). The results of *F* tests were similar to those of AIC analysis (Table 2). AIC values from the 3C models (3C5P and 3C4P) were lower than those from the 2C3P model in all mice, and differences were significant, except for one mouse with A431 ($P < 0.001$). The quality of curve fitting with different models was evaluated, and the results are shown in Figure 5.

Correlation matrices for the 3C5P model are shown in Table 3. K_1/k_2 and k_3 were found to be highly correlated with each other in both tumor cell lines. In LLC, k_3 and k_4 were highly correlated. Because a high level of covariance between microparameters indicates difficulties in independent estimation, K_{FLT} values obtained from the different compartment models were further analyzed. As was expected, K_{FLT} values estimated with 3C5P were much higher than those estimated with 3C4P or GPGA (Table 1). On average, K_{FLT} values were underestimated by approximately 33% (range, −48% to −17%) for A431 tumors and by 56% (range, −69% to −39%) for LLC tumors when k_4 was set to 0 (3C4P vs. 3C5P). K_{FLT} values estimated with GPGA were also consistently lower than those estimated with the 3C5P model (for A431: mean = −26% and range = −38% to −11%; for LLC: mean = −67% and range = −80% to −53%). K_{FLT} composed of microparameters ($K_1 \sim k_3$) was found to be better correlated with k_3 than K_1, as shown in Figure 6.

Correlation of Model Parameters with % Ki-67 and ^{18}F-FLT Phosphorylation

A431 and LLC tumors showed markedly different levels of quantitative and semiquantitative parameters related to ^{18}F-FLT metabolism (k_3, K_{FLT}, and DV_m) ($P < 0.01$) (Table 1). In addition, significant differences in SUVs were noted between the 2 tumor types (6.95 ± 1.14 for A431 and 0.13 ± 0.04 for LLC) and % Ki-67 (81.5 ± 4.4 for A431 and 58.7 ± 6.3 for LLC) ($P < 0.01$).

The radiochromatograms of A431 tumors obtained 2 h after ^{18}F-FLT injection showed that the major radioactive component, which corresponded to phosphorylated ^{18}F-FLT, eluted at a retention time of 2–3 min. No other radioactive peaks were identified. On the other hand, the radiochromatograms of LLC tumors did not contain well-identified peaks. In some tumors, a major peak corresponding to phosphorylated ^{18}F-FLT and a minor peak corresponding to intact ^{18}F-FLT were identified at retention times of 9–10 min. Although fractions of these 2 components were not measured, the results of radio-HPLC were in qualitative agreement with the

TABLE 1
Kinetic Parameters for ^{18}F-FLT PET in Mice Implanted with A431 and LLC Tumors

Cell line	Method	K_1	K_1/k_2	k_3	k_4	V_b	DV_m	K_{FLT}
A431 (n = 7)	3C5P	0.227 (24.6)	1.860 (51.5)	0.123 (32.4)	0.011 (27.6)	0.033 (58.5)	20.64 (46.6)	0.103 (14.2)
	3C4P	0.163 (17.0)	6.349 (35.2)	0.021 (38.7)	—	0.055 (60.2)	—	0.068 (18.1)
	2C3P	0.134 (14.4)	17.52 (34.7)	—	—	0.087 (57.7)	—	—
	GPGA	—	—	—	—	—	—	0.076 (15.6)
LLC (n = 10)	3C5P	0.169 (26.9)	0.656 (14.2)	0.017 (29.3)	0.015 (22.1)	0.044 (45.6)	0.793 (39.9)	0.010 (20.3)
	3C4P	0.133 (28.5)	0.788 (9.4)	0.006 (30.3)	—	0.059 (39.0)	—	0.005 (34.2)
	2C3P	0.063 (24.5)	1.156 (17.7)	—	—	0.093 (15.9)	—	—
	GPGA	—	—	—	—	—	—	0.003 (34.9)

3C5P = 3 compartments and 5 parameters (K_1, K_1/k_2, k_3, k_4, and V_b); 3C4P = 3 compartments and 4 parameters (K_1, K_1/k_2, k_3, and V_b), with k_4 fixed at zero; 2C3P = 2 compartments and 3 parameters (K_1, K_1/k_2, and V_b); GPGA = Gjedde–Patlak graphic analysis.
Data are presented as means (CVs).

TABLE 2
Comparison of Kinetic Models for ^{18}F-FLT PET in Mice Implanted with A431 and LLC Tumors by Use of AIC and Extra Sum-of-Squares *F* Test

Cell line	Mouse	AIC		Change in AIC (1 − 2)	*F* ratio (1 vs. 2)	*P*
		3C5P (1)	3C4P (2)			
A431	1	354.9	389.4	−34.5	2.52	0.005
	2	316.5	364.0	−47.4	3.58	<0.001
	3	399.4	402.2	−2.8	1.07	0.424
	4	345.0	370.9	−25.9	2.00	0.027
	5	340.0	376.2	−36.2	2.64	0.004
	6	303.9	323.5	−19.6	1.69	0.071
	7	320.0	368.3	−48.3	3.66	<0.001
LLC	1	322.1	371.7	−49.6	3.79	<0.001
	2	302.5	331.9	−29.4	2.20	0.014
	3	329.7	369.7	−40.0	2.92	0.002
	4	318.3	361.0	−42.6	3.14	0.001
	5	319.2	351.5	−32.3	2.38	0.008
	6	328.7	348.4	−19.7	1.69	0.070
	7	317.0	353.0	−36.0	2.63	0.004
	8	333.6	382.8	−49.2	3.76	<0.001
	9	325.5	363.1	−37.6	2.74	0.003
	10	334.3	355.9	−21.6	1.78	0.053

percentages of intracellular metabolites of ^{18}F-FLT (90.3% ± 2.8% for A431 and 65.5% ± 8.7% for LLC) relative to total metabolites and dephosphorylated ^{18}F-FLT, as determined by compartmental analysis.

The correlation coefficients for the ^{18}F-FLT PET parameters obtained with the 3C5P model and 120 min of data and % Ki-67 are summarized in Table 4. K_{FLT} (Fig. 7) and k_3 were found to be highly correlated with % Ki-67 ($\rho > 0.8$). Furthermore, the distribution volume ratio (k_3/k_4) between ^{18}F-FLT phosphorylated nucleotides and exchangeable tissue compartment, DV_m, DV_{tot}, and SUV were also highly correlated ($\rho > 0.6$) with % Ki-67. However, K_1 and K_1/k_2 were relatively poorly correlated with % Ki-67.

Feasibility of Simple Models

We compared K_{FLT} values obtained with the 3C5P model and PET data obtained over 60, 90, and 120 min from the initiation of scanning. For A431 tumors, which showed a sufficiently wide K_{FLT} range for correlation analysis, high correlations were found for K_{FLT} values obtained from 120-min and shorter (60- or 90-min) scans by nonlinear regression analysis (3C5P and 3C4P models) (Table 5). However, undesirable negative correlations were obtained for 60- and 120-min scans for LLC tumors (Table 5). GPGA provided a simple estimate of K_{FLT} without complex nonlinear curve fitting, but it had estimation bias when compared with the 3C5P model, mainly because of the assumption of irreversible ^{18}F-FLT metabolism (Table 1). Although K_{FLT} values estimated with GPGA and 60- or 90-min data showed a significant correlation with K_{FLT} values obtained with the 120-min 3C5P model for LLC tumors, this correlation was insignificant for A431 tumors (Table 5). SUVs at 80–90 min and 50–60 min showed lower correlations with K_{FLT} values obtained with the 120-min 3C5P model for both tumor types.

K_{FLT} values obtained with the 3C5P model and 60- or 90-min data were consistently higher than 120-min estimates for both cell lines (Table 6). K_{FLT} values obtained with the 90-min 3C5P model for A431 tumors showed a less than 5% mean difference from those obtained with the 120-min 3C5P model. K_{FLT} values obtained with 3C4P and GPGA and 60- or 90-min data were underestimated, although the 3C4P model showed a high correlation for both tumor types (Tables 5 and 6). The correlations between the K_{FLT} values obtained with the different models and % Ki-67 are shown in Table 7. K_{FLT} values obtained with 60- or 90-min data showed a high correlation with % Ki-67, as did K_{FLT} values obtained with the 3C5P model and 120-min data (Table 4).

DISCUSSION

In the present study, we evaluated the validity of an image-derived LV input function in mouse ^{18}F-FLT PET and investigated tracer kinetic models of ^{18}F-FLT in mice bearing A431 and LLC tumors. The study revealed that the image-derived arterial input function is feasible for ^{18}F-FLT PET kinetic modeling studies in mice with a simple partial-volume correction and that the 3-compartment model with reversible phosphorylation is most suitable for characterizing the kinetics of ^{18}F-FLT in mice. High correlations of K_{FLT} and k_3 with % Ki-67 were found, a result supporting the notion that these ^{18}F-FLT kinetic parameters in mouse tumor models estimate tumor proliferation.

Input Function

Quantitative analysis of dynamic PET images with tracer kinetic modeling requires an arterial plasma input function. However, because of small blood vessel diameters and total blood volumes, serial sampling of arterial blood to measure blood activity in mice is difficult (*15*). Several methods have

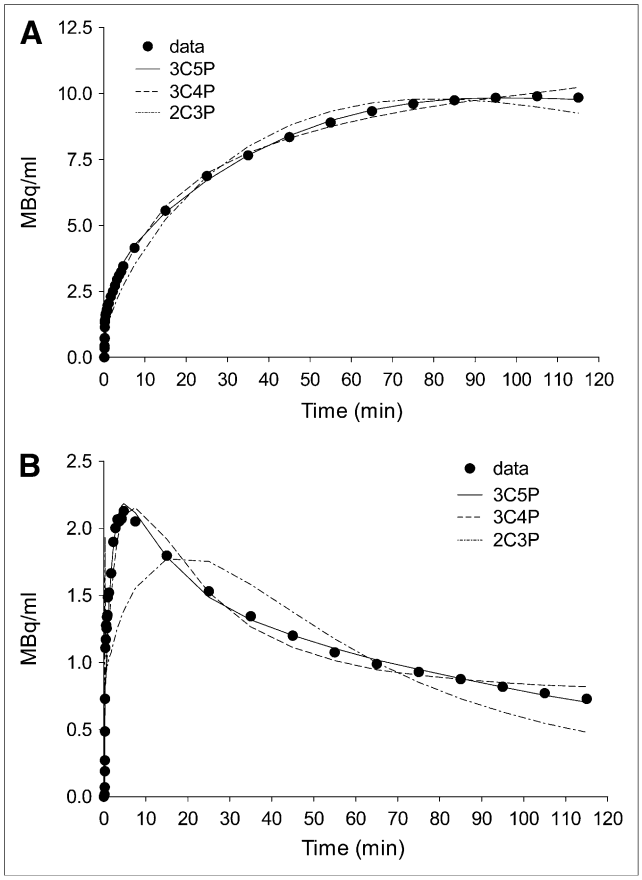

FIGURE 5. Quality of curve fitting obtained with different models and 120 min of data for A431 (A) and LLC (B) tumors. Regression curves defined by 3C5P model were close to data points and did not deviate systematically from data.

been proposed to measure input functions in mice (*24–27*). Automated blood-sampling devices dedicated to small-animal imaging can be used (*24*), but these techniques are limited for multiple-tracer or repetitive studies in the same animals. Image-derived input functions for mouse left ventricles are an alternative to direct blood sampling. This method is attractive, especially in longitudinal studies,

TABLE 3
Average Correlation Coefficients for ^{18}F-FLT Kinetic Parameters in Mice Implanted with A431 and LLC Tumors

Cell line	Parameter	V_b	K_1	K_1/k_2	k_3	k_4
A431	V_b	1	—	—	—	—
	K_1	−0.39	1	—	—	—
	K_1/k_2	0.29	−0.79	1	—	—
	k_3	−0.20	0.67	−0.98	1	—
	k_4	0.10	−0.02	−0.41	0.58	1
LLC	V_b	1	—	—	—	—
	K_1	−0.48	1	—	—	—
	K_1/k_2	0.01	−0.19	1	—	—
	k_3	0.01	0.16	−0.95	1	—
	k_4	−0.03	0.13	−0.83	0.96	1

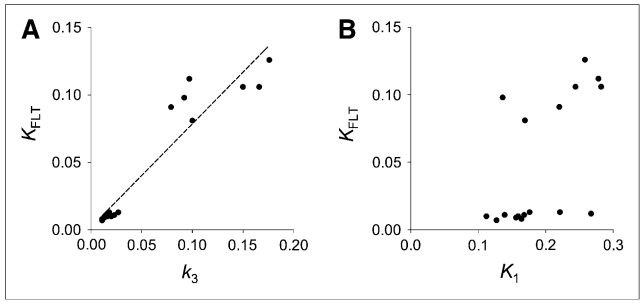

FIGURE 6. Relationships between k_3 and K_{FLT} ($r = 0.95$, $P < 0.0001$) (A) and K_1 and K_{FLT} (B) for both cell lines ($n = 17$). K_{FLT} was better correlated with k_3 than with K_1 (flow-dependent parameter).

because of its noninvasive nature. Moreover, considerable improvements in the spatial resolution and sensitivity of state-of-the-art animal PET systems can increase the accuracy of such measurements.

Therefore, we evaluated the validity of image-derived input functions for mouse left ventricles. Rapid equilibration of ^{18}F-FLT between plasma and whole blood was observed at 30 s after injection, a result indicating that simple image-derived whole-blood activities from left ventricles can be used. In addition, no ^{18}F-FLT metabolite was observed until 2 h after ^{18}F-FLT injection. The observed low levels of ^{18}F-FLT metabolites in mouse plasma agree with the findings of a previous study (*3*) and are probably explained by the relatively low uptake and glucuronidation of ^{18}F-FLT in mouse liver (*3,18,28*).

In the present study, a high correlation between arterial blood sample data and PET data was observed, as shown in Figure 3, and the CVs of the ratios of PET data to blood sample data were less than 15%. Actual intersubject variations of this ratio can be expected to be small because blood sampling and PET measurement errors also contribute to these variations. Therefore, these blood activity analysis results suggest that image-derived LV input functions obtained with a state-of-the-art high-resolution rodent PET

TABLE 4
Correlations Between ^{18}F-FLT PET Parameters Obtained from 3C5P Model and 120 Minutes of Data and % Ki-67

Parameter	Spearman ρ for % Ki-67
K_1	0.47
K_1/k_2	0.59*
k_3	0.86†
k_4	−0.40
k_3/k_4	0.77†
K_{FLT}	0.81†
DV_m	0.74†
DV_{tot}	0.68†
SUV	0.62†

*$P < 0.05$.
†$P < 0.01$.

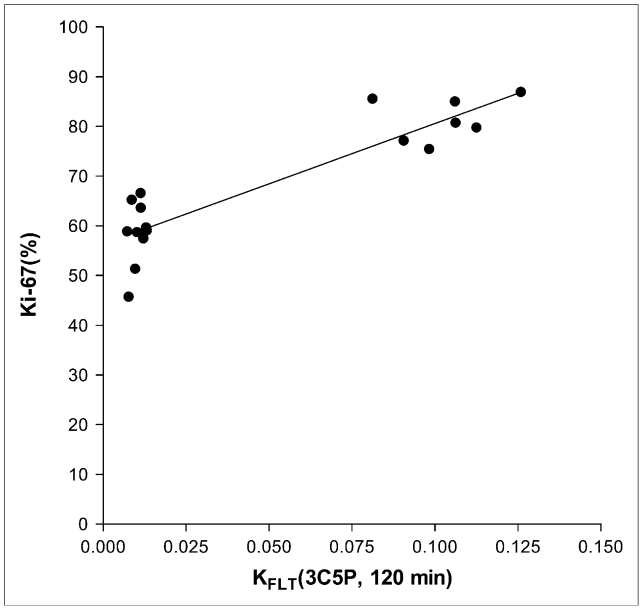

FIGURE 7. Relationship between K_{FLT} values obtained from 3C5P model and 120 min of data and % Ki-67.

scanner can be used for kinetic modeling of ^{18}F-FLT metabolism in mice.

For investigators who plan to use animals of different sizes or different scanners, a correction factor different from that used in the present study should be obtained because the correction factor is dependent on the spatial resolution of the scanner and the LV size of the animal. If ^{18}F-FLT PET is used for treatment monitoring, then change over time is a primary concern, and such a correction factor can be ignored for simplicity.

Compartmental Modeling

In human PET data, phosphorylated ^{18}F-FLT dephosphorylates more slowly than TK1 activity (*29*). As shown in Table 1, dephosphorylation rates (k_4) were also low in the present study and were similar for the 2 tumor cell lines. However, the phosphorylation rate (k_3) in LLC cells was not as rapid as that in A431 cells and was similar to the dephosphorylation rate. Thus, LLC had a low level of ^{18}F-FLT retention, as shown in Figure 4. This finding suggests that k_4 should not be ignored in the kinetic modeling of the LLC cell line when 120 min of data are used. K_{FLT}, which was calculated on the basis of the assumption that k_4 can be ignored, was underestimated by 69% in this cell line (Table 1). A significant loss of phosphorylated ^{18}F-FLT nucleotides was also evident in kinetic studies of non–small cell lung cancer (*11*) and gliomas (*12*). However, previous ^{18}F-FLT kinetic studies in dogs bearing non-Hodgkin's lymphoma and soft-tissue sarcoma (*30*) and in patients with colorectal cancer (*9*) demonstrated that the incorporation of $k_4 \neq 0$ is not necessary to improve model accuracy. In these studies, dynamic PET scans were acquired for only up to 60 min, a length of time that might not have been sufficient to accurately estimate the effects of the k_4 parameter. Further systemic investigation of the issue of $k_4 \neq 0$ in ^{18}F-FLT kinetics is necessary because there are nonbiochemical factors that can lead to better curve fitting with $k_4 \neq 0$. Heterogeneity of tissue composition is an example of such a factor.

In the present study, all compartment models had lower AIC values when the blood volume fraction term was included; this finding means that this parameter should not be neglected in ^{18}F-FLT kinetic models. Blood volume fractions also showed wide variations in both tumor cell lines (Table 1), a result that may have been attributable, in part, to variable vasculature changes in tumors. In addition, tumor-bearing regions showed higher blood volume fractions than did

TABLE 5
Correlations Among ^{18}F-FLT Parameter Estimates Obtained from Different Models

Method	Spearman ρ for K_{FLT}, 3C5P, 120 min	
	A431 (n = 7)	LLC (n = 10)
K_{FLT}, 3C5P, 90 min	0.98*	0.82*
K_{FLT}, 3C5P, 60 min	1.00*	−0.69†
K_{FLT}, 3C4P, 60 min	0.88*	0.91*
K_{FLT}, GPGA, 90 min	0.39	0.90*
K_{FLT}, GPGA, 60 min	0.56	0.83*
SUV, 80–90 min	0.39	−0.09
SUV, 50–60 min	0.39	−0.29

*$P < 0.01$.
†$P < 0.05$.

TABLE 6
Average Percentage Changes in ^{18}F-FLT Net Influx Parameters (K_{FLT}) Obtained from 3C5P Model and 120 Minutes of Data

Method	Mean ± SD % change	
	A431 (n = 7)	LLC (n = 10)
3C5P, 90 min	4.2 ± 3.4	27 ± 18.1
3C5P, 60 min	15.2 ± 5	100.5 ± 64.3
3C4P, 60 min	−18 ± 6.3	−35.1 ± 6.8
GPGA, 90 min	−26.1 ± 9.8	−63.4 ± 7.7
GPGA, 60 min	−18.6 ± 7.6	−56.6 ± 8.3

TABLE 7
Correlations Between K_{FLT} Values Obtained from Different Models and % Ki-67

Method	Spearman ρ for % Ki-67*
3C5P, 90 min	0.77
3C5P, 60 min	0.76
3C4P, 60 min	0.80
GPGA, 90 min	0.72
GPGA, 60 min	0.73

*$P < 0.01$ for all values.

normal regions, a result that is probably associated with enhanced neovascularization in these tumor models (*31*). With regard to the use of ^{18}F-FLT PET for the assessment of therapeutic outcomes, considerations of blood volume fractions are important because of the possible effects of increased edema induced by treatment (*13*).

Model Parameters

K_{FLT} and k_3 showed high correlations with % Ki-67, but no correlation of K_1 and k_4 with % Ki-67 was observed (Table 4). The strong correlation of K_{FLT} with % Ki-67 seems to be related to the parameter k_3, which is directly associated with TK1 activity, because K_{FLT} is not flow-dependent (Fig. 6) and K_1 levels were similar between the 2 tumor models. Better correlations between k_3 or K_{FLT} and % Ki-67 than between SUVs and % Ki-67 may be attributable to a significant amount of label loss because of dephosphorylation (k_4) and better normalization of tumoral activity by input function integration rather than use of the injected dose.

In general, macroparameters, that is, combinations of microparameters, were more stable than individual microparameters. Therefore, associations between several macroparameters (k_3/k_4, K_{FLT}, DV_m, and DV_{tot}) and ^{18}F-FLT metabolism were explored in the present study. Although all were found to be useful for differentiating A431 tumors and LLC tumors, K_{FLT} values in tumor-bearing regions had the smallest variability, as shown in Table 1. In addition, K_{FLT} showed a strong correlation with k_3 (Fig. 6).

Simple Models

Our results show that PET parameters (k_3 and K_{FLT}) estimated with the 3C5P model and 120 min of PET data reflect well the metabolism of ^{18}F-FLT in tumor cells. However, PET of mice for 120 min is inconvenient because of the time involved and the possibility of animal movement. The possible biologic effects of long-term anesthesia are also problematic.

Unfortunately, K_{FLT} estimates based on the 60- or 90-min 3C5P model were consistently higher than K_{FLT} estimates based on the 120-min model, and those obtained from the 3C4P model were lower. Only in tumor models with high uptake (A431 models) did 90-min K_{FLT} estimates differ from 120-min estimates by less than 5%. This result suggests that the estimation of k_4 is a vital element and that 60-min data are inappropriate in these tumor models if the absolute quantification of K_{FLT} is important.

If the specific aim of an ^{18}F-FLT PET study is to monitor the therapeutic response after cancer treatment, then assessment of relative changes in a kinetic parameter over time will be sufficient. Despite the overestimation of K_{FLT} values, the 60- or 90-min 3C5P model had a strong correlation with the 120-min model in highly proliferative tumor cells (A431). Although K_{FLT} values obtained with the 60-min 3C5P model in LLC tumors had a negative correlation with those obtained with the 120-min 3C5P model and showed a high relative percentage of change, these results were mainly attributable to the fact that LLC tumors have a very low level and narrow range of K_{FLT} values; these conditions are not appropriate for these comparisons. In addition, K_{FLT} values obtained with shorter scan times (60 or 90 min) showed a high correlation with % Ki-67 (Table 7), as did K_{FLT} values obtained with the 3C5P model and 120 min of data. Although there is still controversy regarding the appropriateness of the incorporation of k_4 in an ^{18}F-FLT kinetic analysis with 60 min of data, these experimental results support the notion that a dynamic ^{18}F-FLT PET scan time shorter than 120 min can be used if the only parameter of interest is the relative change in K_{FLT}. In addition, the incorporation of k_4 in a kinetic analysis of shorter scan data seems to be feasible; this factor is important in the accurate estimation of K_{FLT} in therapeutic response monitoring with possibly varying k_4 values (*11*).

K_{FLT} estimates based on the 3C4P model ($k_4 = 0$) and 60 min of data correlated well with those based on the full model and data (3C5P and 120 min), as shown in Table 5, and the level of underestimation of K_{FLT} was not significant. Therefore, this model will also be useful in some applications in which only the relative change in K_{FLT} is important and in which K_{FLT} is insensitive to changes in k_4 or the assumption of no changes in k_4 can be justified.

Limitations

This study has several limitations. First, we used a relatively small number of mice for each tumor model. Nevertheless, consistent results were obtained with respect to model selection and parameter estimation. Second, concentrations of serum thymidine and the lumped constant for ^{18}F-FLT were not considered. Although the consideration of a lumped constant, which accounts for differences in the transport and phosphorylation of ^{18}F-FLT and thymidine, is required, no systematic study of this issue has been undertaken (*32*). Finally, 30–46 MBq of ^{18}F-FLT were injected into mice to analyze ^{18}F-FLT metabolites more accurately in tumors, because initial studies with 7.5 MBq of ^{18}F-FLT did not result in a peak in LLC tumors. However, the effects of a perturbation of cellular proliferation on study results are likely to be negligible.

CONCLUSION

The present study showed that the image-derived arterial input function is feasible for kinetic modeling studies of ^{18}F-FLT PET in mice. For 120-min dynamic PET data, the 3-compartment model with reversible phosphorylation and a variable blood volume fraction was found to best describe tissue time–activity curves in tumor-bearing regions. K_{FLT} values obtained with this model showed reasonable intersubject variability and discrimination ability for tumor models with different proliferation properties. At least 90 min of data are necessary to obtain accurate absolute K_{FLT} values for A431 with the 3C5P model. Our results also suggested that imaging for 60 min is useful in some applications, such as cancer treatment monitoring, in which the

relative change in the K_{FLT} parameter over time is more important than absolute values.

ACKNOWLEDGMENTS

This work was supported by the Real-Time Molecular Imaging Research Program and Basic Research Program (R01-2006-000-10296-0) of the Korean Science & Engineering Foundation, the Korea Health 21 R&D Project, the Ministry of Health & Welfare (grant A062254), and the Seoul R&BD Program (grant 10550) managed by the Seoul Development Institute. The authors would like to acknowledge that this study was assisted by the support of the Giga-Network (KREONET) of KISTI.

REFERENCES

1. Sherley JL, Kelly TJ. Regulation of human thymidine kinase during the cell cycle. *J Biol Chem.* 1988;263:8350–8358.
2. Grierson JR, Shields AF. Radiosynthesis of 3′-deoxy-3′-[^{18}F]fluorothymidine: [^{18}F]FLT for imaging of cellular proliferation in vivo. *Nucl Med Biol.* 2000;27:143–156.
3. Barthel H, Cleij MC, Collingridge DR, et al. 3′-Deoxy-3′-[^{18}F]fluorothymidine as a new marker for monitoring tumor response to antiproliferative therapy in vivo with positron emission tomography. *Cancer Res.* 2003;63:3791–3798.
4. Wagner M, Seitz U, Buck A, et al. 3′-[^{18}F]Fluoro-3′-deoxythymidine ([^{18}F]-FLT) as positron emission tomography tracer for imaging proliferation in a murine B-cell lymphoma model and in the human disease. *Cancer Res.* 2003;63: 2681–2687.
5. Choi SJ, Kim JS, Kim JH, et al. [^{18}F]3′-Deoxy-3′-fluorothymidine PET for the diagnosis and grading of brain tumors. *Eur J Nucl Med Mol Imaging.* 2005;32: 653–659.
6. Kenny LM, Vigushin DM, Al-Nahhas A, et al. Quantification of cellular proliferation in tumor and normal tissues of patients with breast cancer by [^{18}F]fluorothymidine-positron emission tomography imaging: evaluation of analytical methods. *Cancer Res.* 2005;65:10104–10112.
7. Waldherr C, Mellinghoff IK, Tran C, et al. Monitoring antiproliferative responses to kinase inhibitor therapy in mice with 3′-deoxy-3′-^{18}F-fluorothymidine PET. *J Nucl Med.* 2005;46:114–120.
8. Muzi M, Mankoff DA, Grierson JR, Wells JM, Vesselle H, Krohn KA. Kinetic modeling of 3′-deoxy-3′-fluorothymidine in somatic tumors: mathematical studies. *J Nucl Med.* 2005;46:371–380.
9. Visvikis D, Francis D, Mulligan R, et al. Comparison of methodologies for the in vivo assessment of 18FLT utilisation in colorectal cancer. *Eur J Nucl Med Mol Imaging.* 2004;31:169–178.
10. Jacobs AH, Thomas A, Kracht LW, et al. ^{18}F-Fluoro-L-thymidine and ^{11}C-methylmethionine as markers of increased transport and proliferation in brain tumors. *J Nucl Med.* 2005;46:1948–1958.
11. Muzi M, Vesselle H, Grierson JR, et al. Kinetic analysis of 3′-deoxy-3′-fluorothymidine PET studies: validation studies in patients with lung cancer. *J Nucl Med.* 2005;46:274–282.
12. Muzi M, Spence AM, O'Sullivan F, et al. Kinetic analysis of 3′-deoxy-3′-^{18}F-fluorothymidine in patients with gliomas. *J Nucl Med.* 2006;47:1612–1621.
13. Schiepers C, Chen W, Dahlbom M, Cloughesy T, Hoh CK, Huang SC. ^{18}F-fluorothymidine kinetics of malignant brain tumors. *Eur J Nucl Med Mol Imaging.* 2007;34:1003–1011.
14. Hume SP, Myers R. Dedicated small animal scanners: a new tool for drug development? *Curr Pharm Des.* 2002;8:1497–1511.
15. Pomper MG, Lee JS. Small animal imaging in drug development. *Curr Pharm Des.* 2005;11:3247–3272.
16. Kim TJ, Ravoori M, Landen CN, et al. Antitumor and antivascular effects of AVE8062 in ovarian carcinoma. *Cancer Res.* 2007;67:9337–9345.
17. Lee JS, Orita H, Gabrielson K, et al. FDG-PET for pharmacodynamic assessment of the fatty acid synthase inhibitor C75 in an experimental model of lung cancer. *Pharm Res.* 2007;24:1202–1207.
18. Sugiyama M, Sakahara H, Sato K, et al. Evaluation of 3′-deoxy-3′-^{18}F-fluorothymidine for monitoring tumor response to radiotherapy and photodynamic therapy in mice. *J Nucl Med.* 2004;45:1754–1758.
19. Oyama N, Ponde DE, Dence C, Kim J, Tai YC, Welch MJ. Monitoring of therapy in androgen-dependent prostate tumor model by measuring tumor proliferation. *J Nucl Med.* 2004;45:519–525.
20. Yang YJ, Ryu JS, Kim SY, et al. Use of 3′-deoxy-3′-[^{18}F]fluorothymidine PET to monitor early responses to radiation therapy in murine SCCVII tumors. *Eur J Nucl Med Mol Imaging.* 2006;33:412–419.
21. Lee SJ, Oh SJ, Chi DY, et al. Simple and highly efficient synthesis of 3′-deoxy-3′-[^{18}F]fluorothymidine using nucleophilic fluorination catalyzed by protic solvent. *Eur J Nucl Med Mol Imaging.* 2007;34:1406–1409.
22. Kim JS, Lee JS, Im KC, et al. Performance measurement of the microPET Focus 120 scanner. *J Nucl Med.* 2007;48:1527–1535.
23. Burger C, Buck A. Requirements and implementation of a flexible kinetic modeling tool. *J Nucl Med.* 1997;38:1818–1823.
24. Wu HM, Sui G, Lee CC, et al. In vivo quantitation of glucose metabolism in mice using small-animal PET and a microfluidic device. *J Nucl Med.* 2007;48:837–845.
25. Ferl GZ, Zhang X, Wu HM, Huang SC. Estimation of the ^{18}F-FDG input function in mice by use of dynamic small-animal PET and minimal blood sample data. *J Nucl Med.* 2007;48:2037–2045.
26. Kim J, Herrero P, Sharp T, et al. Minimally invasive method of determining blood input function from PET images in rodents. *J Nucl Med.* 2006;47:330–336.
27. Laforest R, Sharp TL, Engelbach JA, et al. Measurement of input functions in rodents: challenges and solutions. *Nucl Med Biol.* 2005;32:679–685.
28. Nicolas F, De Sousa G, Thomas P, Placidi M, Lorenzon G, Rahmani R. Comparative metabolism of 3′-azido-3′-deoxythymidine in cultured hepatocytes from rats, dogs, monkeys, and humans. *Drug Metab Dispos.* 1995;23:308–313.
29. Grierson JR, Schwartz JL, Muzi M, Jordan R, Krohn KA. Metabolism of 3′-deoxy-3′-[F-18]fluorothymidine in proliferating A549 cells: validations for positron emission tomography. *Nucl Med Biol.* 2004;31:829–837.
30. Shields AF, Grierson JR, Muzik O, et al. Kinetics of 3′-deoxy-3′-[F-^{18}]fluorothymidine uptake and retention in dogs. *Mol Imaging Biol.* 2002;4:83–89.
31. Myoken Y, Kayada Y, Okamoto T, Kan M, Sato GH, Sato JD. Vascular endothelial cell growth factor (VEGF) produced by A-431 human epidermoid carcinoma cells and identification of VEGF membrane binding sites. *Proc Natl Acad Sci USA.* 1991;88:5819–5823.
32. Barthel H, Aboagye E, Price P. Author reply. *Cancer Res.* 2003;63:8560.